Remote Sensing of Environment 113 (2009) 362–370

Contents lists available at ScienceDirect

Remote Sensing of Environment

journal homepage: www.elsevier.com/locate/rse

Spatial downscaling of TRMM precipitation using vegetative response on the Iberian Peninsula

W.W. Immerzeel [a,*], M.M. Rutten [b], P. Droogers [a]

[a] FutureWater, Costerweg 1G, 6702 AA Wageningen, The Netherlands
[b] Technical University of Delft, Faculty of Civil Engineering and Geosciences, P.O. Box 5048, 2600 GA Delft, The Netherlands

ARTICLE INFO

Article history:
Received 28 July 2008
Received in revised form 2 October 2008
Accepted 4 October 2008

Keywords:
Downscaling
Precipitation
TRMM
NDVI
Iberian Peninsula

ABSTRACT

Precipitation data with accurate, high spatial resolution are crucial for improving our understanding of basin scale hydrology. We explore the relation between precipitation estimates derived from the Tropical Rainfall Monitoring Mission (TRMM) and the normalized difference vegetation index (NDVI) for different spatial scales on the Iberian Peninsula in southern Europe, using time series from 2001 to 2007. Analysis shows that NDVI is a good proxy for precipitation. On an annual basis an exponential function best describes the relation between NDVI and precipitation. The optimum relation between NDVI and precipitation is found at an approximate scale of 75–100 km. This is an intermediate scale and it is likely that at smaller scales NDVI is determined primarily by anthropogenic land use and at larger scales factors such as geology, soils, and temperature play an increasingly important role. The fact that both TRMM and NDVI are subject to bias due to orbital deviations, atmospheric conditions and imperfect retrieval algorithms could also influence the scale dependency. The derived relation between NDVI and precipitation is used to develop a new downscaling methodology that uses coarse scale TRMM precipitation estimates and fine scale NDVI patterns. The downscaled precipitation estimates are subsequently validated using an independent precipitation dataset. The downscaling procedure resulted in significant improvements in correlation, bias, and root mean square error for average annual precipitation over the whole period, for a dry year (2005), and a wet year (2003).

1. Introduction

Precipitation is a major driving force in the water cycle and accurate data with sufficient spatial detail are of key importance in assessing basin scale hydrology. It is common practice that hydrological models are run with precipitation data acquired from a limited number of gauges (Goodrich et al., 1995). Recent studies showed that the spatial resolution greatly influences model outcomes and that models using raster based precipitation data outperform models that use precipitation derived from point measurements (rain gauges). (Guo et al., 2004; Smith et al., 2004). Smith et al. (2004) concluded that for complex basins, which are rarely completely, or uniformly covered by a single precipitation event, the use of distributed rainfall in modelling, resulted in better discharge simulations than modelling with traditional lumped rainfall from point measurements. Schuurmans and Bierkens (2007) also showed that spatial patterns of precipitation are essential in characterizing the behaviour of a catchment. Their study focused on a relatively small catchment (135 km^2) and even at this scale it was concluded that the use of a single rain gauge for rainfall input decreases the accuracy of discharge, groundwater level, and soil moisture predictions. They also concluded that information on the spatial variability of rainfall is required to get insight into the day-to-day spatial variability of discharge, groundwater level, and soil moisture content. Access to reliable high resolution precipitation datasets is therefore highly relevant for hydrological studies.

Remote sensing can provide spatial precipitation patterns. Ground radar systems can also provide spatial precipitation information but validation of ground radar rainfall products is a major challenge for general hydrologic applications (Krajewski and Smith, 2002). Ground radar systems also have a limited range and are generally aimed at monitoring of extreme events over limited time spans, making their use less suitable for long term assessments. Satellite remote sensing is a better source of spatial precipitation data. Such data are generally readily available over longer periods and covers large areas. Many different algorithms and types of sensors aboard a variety of satellites exist. Adler et al. (2001) provide an extensive overview and intercompare 25 satellite based products to four model based, and to two climatological products. In this study we use blended data products from the Tropical Rainfall Monitoring Mission (TRMM) with a high spatial resolution. These products are derived using sophisticated algorithms and are based on data from a range of different sensors (Huffman et al., 2007). These products have a spatial resolution of

* Corresponding author.
E-mail address: w.immerzeel@futurewater.nl (W.W. Immerzeel).

0034-4257/$ – see front matter © 2008 Elsevier Inc. All rights reserved.
doi:10.1016/j.rse.2008.10.004

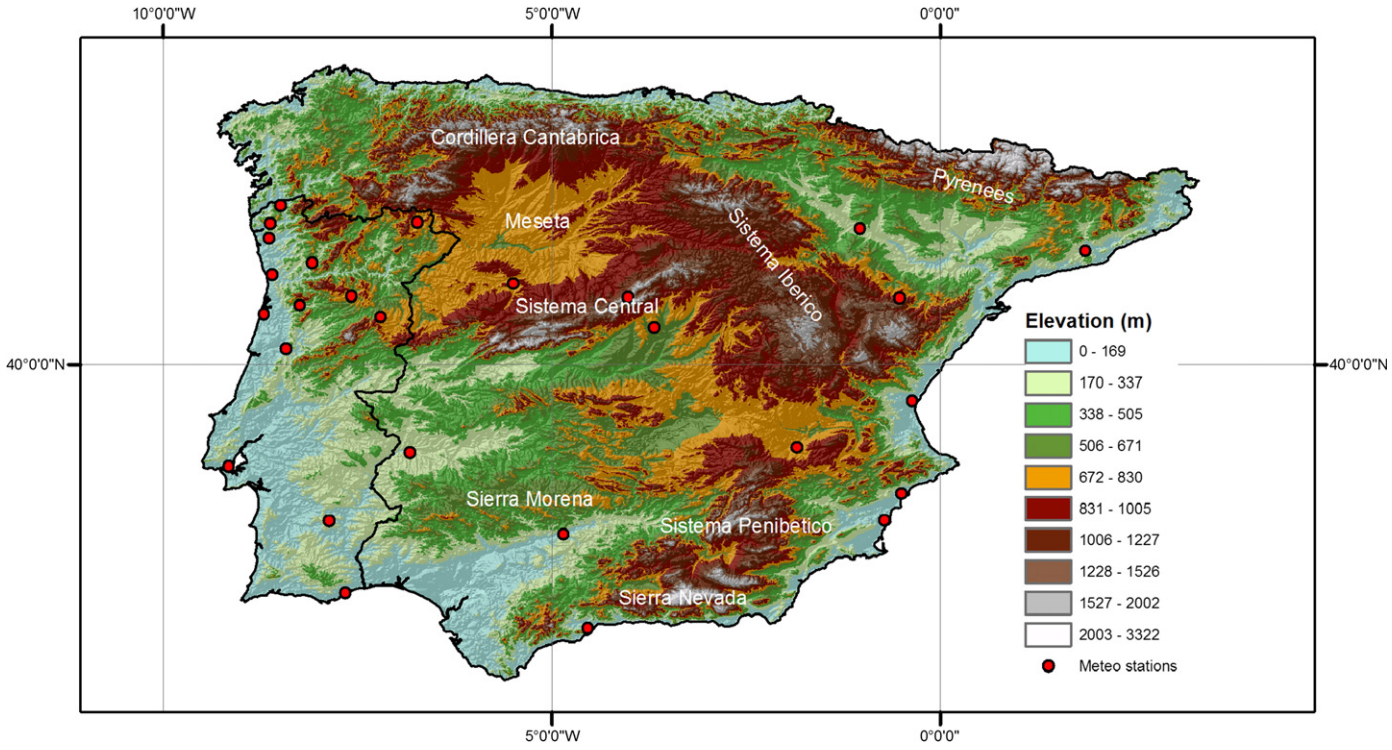

Fig. 1. Study area location, elevation and location of the meteorological stations used for validation.

0.25° and span the globe from 50 °N to 50 °S. Although this resolution is high compared to other satellite based products, it is still too coarse for use in (small) basin scale hydrological studies. A robust downscaling procedure below the pixel resolution would be highly advantageous for such hydrological applications.

In this study we hypothesize that greenness of vegetation is a proxy for cumulative precipitation. To quantify vegetation greenness the normalized difference vegetation index (NDVI, Tucker, 1979) is used. Since NDVI data are generally available at a much higher resolution than precipitation data, NDVI can be used in a downscaling procedure. By linearly aggregating the NDVI data to the spatial scale of the precipitation data a relation between NDVI and precipitation can be established and used to predict cumulative spatial rainfall over catchments at relatively high resolution. This is however not trivial and only allowed if the process scale is larger than the observation scale (Pelgrum, 2000). The scale of typical synoptic mid-latitude weather systems is typical in the range of 1000 km. However at smaller, local scales there is also large variation in precipitation due to mesoscale climatic processes, land use, and relief interactions. These processes causing local precipitation variation typically occur at scales of 2 km and larger (Orlanski, 1975). The scale (extent and spatial distribution) of precipitation is therefore larger than the NDVI scale (1 km) and aggregating NDVI to explain precipitation is therefore legitimate. High resolution NDVI data have previously also been used to sharpen thermal bands (Kustas et al., 2003; Agam et al., 2007). Previous studies (Malo and Nicholson, 1990; Davenport and Nicholson, 1993; Grist et al., 1997; Immerzeel et al., 2005) have also related NDVI behaviour to precipitation, but NDVI has not been used for downscaling satellite based precipitation estimates. In this study, the relation between TRMM precipitation estimates and NDVI is explored for different spatial scales on the Iberian Peninsula (Spain and Portugal) in southern Europe. Based on this assessment, an empirical relationship is defined. This relation is used to develop a new downscaling methodology that uses coarse scale TRMM precipitation estimates and fine scale NDVI patterns. The downscaled precipitation estimate is subsequently validated using an independent dataset from precipitation gauges.

2. Study area

The Iberian Peninsula (IP, Fig. 1) is located in the extreme southwest of Europe, and includes Spain, Portugal, Andorra and Gibraltar and a small part of France. It is bordered by the Mediterranean Sea and the Atlantic Ocean. The Pyrenees form the northeast edge of the Peninsula, separating it from the rest of Europe. The IP has a surface area of 582,860 km^2. Elevation ranges from sea level to 3479 m (Mulhacén in the Sierra Nevada). Fig. 1 clearly shows the Meseta (42 °N, 6 °W), which is a vast plateau in the heart of the IP surrounded by a number of mountain ranges (Sistema Central, Sierra Morena, the Cordillera Cantábrica, and the Sistema Ibérico). Other mountain ranges include the Pyrenees in the north, Sistema Penibético in the southeast and the Sierra Nevada in the south.

The IP has a temperate climate with hot and dry summers in the interior and wetter and cooler summers along the coastlines, especially along the Atlantic coast. Fig. 2 shows the average monthly precipitation and temperature averaged over the entire IP. There is a clear seasonal pattern. July is the warmest month with an average

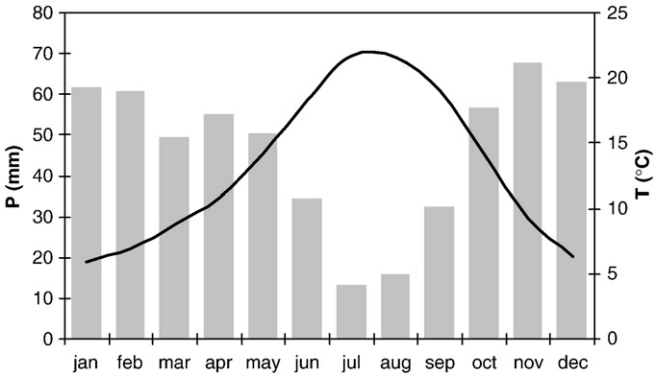

Fig. 2. Average monthly precipitation and temperature for the IP. Bars indicate precipitation and the line indicates temperature.

temperature of 21.7 °C. December is the coldest with an average temperature of 6.4 °C. Precipitation is highest in November (68 mm) and lowest in July (13 mm). Average annual precipitation equals 562 mm. The distribution of precipitation on the IP shows strong gradients, with higher values in the west and the north of the IP (>1000 mm year^{-1}) and lower values toward the southeast (<400 mm year^{-1}). The southeast also shows the highest variation in precipitation. Large parts of the IP are semi-arid. Annual precipitation is related to large scale circulation indices (North Atlantic Oscillation, East Atlantic and the Southern Oscillation Index) (Rodriguez-Puebla et al., 1998).

3. Methodology

3.1. Datasets

3.1.1. Tropical Rainfall Monitoring Mission

The Tropical Rainfall Monitoring Mission (TRMM) is a joint project between NASA and the Japanese space agency, JAXA. TRMM was launched on November 27th, 1997. The primary TRMM instruments are the Precipitation Radar (PR) (the first and only rain radar in space) and the TRMM Microwave Imager (TMI), a multi-channel passive microwave radiometer, which complements the PR by providing total hydrometeor (liquid and ice) content within precipitating systems. The Visible Infrared Scanner (VIRS) is used to provide the cloud context of the precipitation and is used to connect microwave precipitation information to infrared-based precipitation estimates from geosynchronous satellites. TRMM processing algorithms combine information from these instruments and provide the finest scale (0.25°×0.25°) precipitation estimate currently available from space (Huffman et al., 2007). A range of orbital and gridded TRMM products are available and in this study the 3B42 and 3B43 products are used.

The 3B42 estimates are routinely produced in four stages:

- The microwave precipitation estimates are calibrated and combined at three-hourly intervals at a resolution of 0.25°. Passive microwave estimate from AMSR-E, AMSU-B and SSM/I are also used in this step. All passive microwave estimates are calibrated using the TRMM combined instrument precipitation estimate (2B31).
- Infrared precipitation estimates are generated using the calibrated microwave precipitation.
- The microwave and IR estimates are combined.
- All three-hourly data are aggregated to monthly values.

Huffman et al. (2007) provide detailed information on the different processing steps. The 3B42 precipitation is a multi-satellite product. The 3B42 product is combined with gauge precipitation data as described by Huffman et al. (1997). The gridded precipitation gauge based product (1°×1°) of the Global Precipitation Climatological Center (Rudolf, 1993) is used to perform a large scale bias correction on the 3B42 product similar to the method described by Huffman et al. (1997). The resulting monthly product, which is a combination of satellite and gauge data, is the 3B43 product.

For this study, monthly 3B42 and 3B43 data from 2001–2007 are available through the GES-DISC Interactive Online Visualization ANd aNalysis Infrastructure (Giovanni) as part of the NASA's Goddard Earth Sciences (GES) Data and Information Services Center (DISC).

3.1.2. SPOT VEGETATION

The VEGETATION instrument (VGT), on board the SPOT 4 and SPOT 5 satellites has four spectral bands: blue (0.43–0.47 μm), red (0.61–0.68 μm), Near InfraRed (NIR, 0.78–0.89 μm) and Short Wave InfraRed (SWIR, 1.58–1.74 μm). The red and NIR bands are used to calculate NDVI ([NIR−RED]/[NIR+RED]). The spatial resolution of the imagery is 1 km at nadir and the 2200 km swath width allows daily imaging of about 90% of the equatorial regions, the remaining 10% being imaged the following day. At latitudes higher than 35° (North and South), all regions are observed daily. The synthesized pre-processed S10 NDVI product was used in this study, which is a geometrically and radiometrically corrected 10-day composite image. The 10 day-periods were defined from the 1st to the 10th, from the 11th to the 20th and from the 21st to the end of each month. Atmospheric corrections were performed using the Simplified Method for Atmospheric Corrections (SMAC) (Rahman and Dedieu, 1994).

In this study a dataset containing 252 (7 years×36 images per year) 10-day composite NDVI images spanning the period January 2001 to December 2007 was used. From January 2001 to January 2003 data from the VGT1 sensor aboard the SPOT-4 satellite were used and from February 2003 onwards data from the VGT2 sensor aboard the SPOT-5 satellite were used. Both sensors have the same spectral and spatial properties. For more information on the VGT instrument see the VEGETATION User Guide (http://www.spot-vegetation.com). A spatial subset of the imagery was made using the IP boundaries, and annual NDVI images were calculated by averaging the 36 10-day composites.

3.1.3. Meteorological data

A dataset with daily station data in Europe was used for validation of the downscaled precipitation grids. This dataset was generated as part of the European Climate Assessment (ECA) project and described by Klein Tank et al. (2002). For the IP the dataset contains a total of 28 meteorological stations, which are shown in Fig. 1.

3.2. Downscaling

The TRMM datasets were downscaled using an approach developed by Agam et al. (2007) for sharpening thermal imagery with NDVI. The approach is based on the assumption that a relation exists between NDVI and precipitation at different scales. This relation is then used at a finer scale to generate more detail in the precipitation grids. A stepwise approach was used to test the assumption. First the average NDVI from 2001–2007 was compared to the accumulated average annual 3B42 and 3B43 precipitation for the same period at different resolutions (0.25°, 0.50°, 0.75°, 1.00° and 1.25°). The NDVI data, with an original resolution of 1 km, were scaled up using grid cell averaging. For each resolution, the NDVI values were regressed against the TRMM precipitation. The best fit among the different resolutions was used in the downscaling procedure. As a second step, the validity of the regression relationships was tested for individual years. The wettest year (2003) and the driest year (2005) were selected from the 2001–2007 time series.

Downscaling was performed as follows. A distinction was made between the low resolution (LR) and the high resolution (HR) imagery. HR refers to the resolution of the original NDVI imagery (1 km) and LR refers to the five different resolutions which are tested starting at the nominal 3B43 resolution (0.25°). An exponential regression was performed between $NDVI_{LR}$ and the TRMM product, which is expressed in the function below (Eq. (1)).

$$P_e(NDVI_{LR}) = a \cdot e^{b \cdot NDVI_{LR}} \quad (1)$$

Where P_e (mm year^{-1}) is the TRMM estimate based on $NDVI_{LR}$ and a and b are the fitting coefficients resulting from the regressions between NDVI and 3B43 at different scales. This was repeated for all five low resolutions and the resolution with the best fit was used in the downscaling procedure. Then the difference between P_e and the TRMM precipitation ($\Delta TRMM_{LR}$) was calculated at the nominal 0.25° resolution (LR) according to Eq. (2).

$$\Delta TRMM_{LR} = 3B43 - P_e(NDVI_{LR}) \quad (2)$$

This low resolution residual was interpreted as the amount of rainfall that cannot be explained by the NDVI regression function. Using the centre points of the TRMM grid cells the $\Delta 3B43_{LR}$ was interpolated to HR ($\Delta TRMM_{HR}$) using a simple spline tension

interpolator (Franke, 1982). Splining is a deterministic technique to represent two dimensional curves on three dimensional surfaces (Eckstein, 1989; Hutchinson and Gessler, 1994). The mathematical spline function is constrained at the centre points of the TRMM grid cells, it assumes smoothness of variation, and is typically used for regularly-spaced data.

The next step was to estimate the precipitation at high resolution (1 km) according to

$$P_e(\mathrm{NDVI_{HR}}) = a \cdot e^{b \cdot \mathrm{NDVI_{HR}}} \quad (3)$$

The final downscaled product (P_{ds}) was calculated by adding the HR residual ($\Delta\mathrm{TRMM_{HR}}$) to the HR precipitation estimate based on the NDVI according to

$$P_{ds} = P_e(\mathrm{NDVI_{HR}}) + \Delta\mathrm{TRMM_{HR}} \quad (4)$$

The above can be summarized as a two step approach. Firstly, an exponential relation between the low resolution NDVI and precipitation is derived at an optimum scale between 0.25° and 1.25°. Secondly, the high resolution precipitation field is derived using this relation, the high resolution NDVI and the interpolated residual, which compensates for precipitation variation not explained by NDVI.

We have refined the downscaling methodology as described by Agam et al. (2007) in two ways:

- The relation between NDVI and precipitation was tested at different resolutions and we have selected the basis function at an optimum resolution with the highest r^2.
- The residuals were interpolated using a spline interpolator.

3.3. Validation

The downscaled precipitation for the wet year, the dry year, and the 2001–2007 average was validated using the daily station datasets. For the 3B42, 3B43 and P_{ds} a number of commonly used performance indicators were calculated (Hoffmann et al., 2004).

Firstly, the coefficient of determination (r^2) between the station data and the precipitation product was calculated. A value of one corresponds to a perfect correlation and a value of zero indicates that the station data and the precipitation product are uncorrelated.

Secondly, the bias (B) was determined, which is expressed as

$$B = \frac{\sum_{i=1}^{n} M_i}{\sum_{i=1}^{n} O_i} - 1 \quad (5)$$

Where M is the 3B42, 3B43 or P_e at the station location, O is the observed station precipitation, i the index of the station number and n the total number of stations. The bias indicates the degree to which the observed value is over or underestimated.

Finally, the root mean square error (RMSE) was assessed by means of the equation

$$\mathrm{RMSE} = \left(\sum_{i}^{n} (O_i - M_i)^2 / n \right)^{1/2} \quad (6)$$

4. Results and discussion

4.1. NDVI and TRMM regression

Fig. 3 shows the average annual NDVI and 3B43 accumulated annual precipitation for the period 2001–2007. Fig. 3 reveals that precipitation in the northern and north western part along the Atlantic Ocean is indeed much higher (~1200 mm y^{-1}) than in central and south eastern Spain (~400 mm y^{-1}). The relatively dry Meseta is also clearly visible as well as the higher precipitation in the major mountain ranges across the IP. NDVI shows a very similar pattern as 3B43 precipitation and a clear spatial correlation exists between the two datasets.

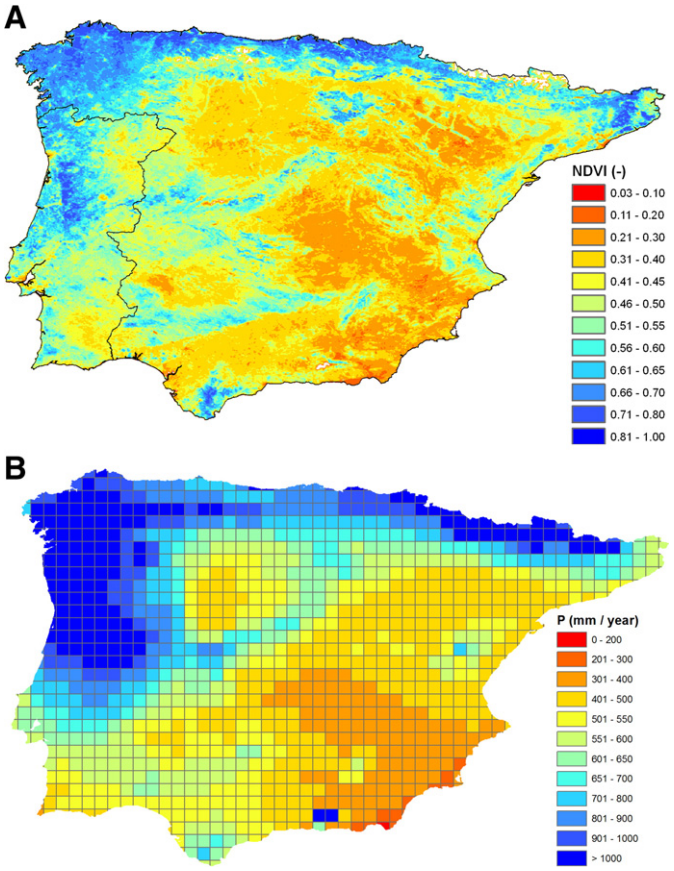

Fig. 3. Average annual NDVI (1 km resolution) (A) and 3B43 accumulated annual precipitation (0.25° resolution) (B) for the period 2001–2007.

The scale dependency of the NDVI and 3B43 relationship was tested at different spatial resolutions. Fig. 4 shows the results of fitting exponential functions at the six different resolutions. Fig. 4 shows that at all resolutions a clear relationship exists between the greenness of vegetation and precipitation. The curves show that the relationships hold only to high NDVI values where the relation with precipitation dissipates and water is not limiting growth anymore. The strongest relation is found in the NDVI range between 0.2 and 0.7 and in the precipitation range from 200–800 mm y^{-1}. Given that the precipitation over the majority of the IP falls in this range it is concluded that the NDVI-3B43 relation could be used for downscaling. For the observed data range an exponential function provides the best fit. Other functions were tested at the nominal resolution of 0.25°, but resulted in lower r^2 values (linear = 0.52, power function = 0.55, 2nd order polynomial = 0.53). There were differences in the function fitting coefficients for the different resolutions. The r^2 ranged from 0.57 (0.25°) to 0.75 (0.75°). When aggregating to a lower resolution the coefficient of determination increased and there was a peak at 0.75° and then a slow decrease in correlation at even lower resolutions. There was an optimum scale at which we found the best relation between the NDVI and 3B43. At this optimum scale, precipitation was better explained by NDVI than at any other scale. The NDVI was at this scale least influenced by factors such as geology, soils, vegetation type, temperature, irrigation, and anthropogenic influences. By using this optimum fit at a smaller resolution we estimated the local precipitation assuming a similar response as at the optimum scale. Note that the differences in the a and b coefficient of the exponential curves for the different scales are not very large, and a similar relation between NDVI

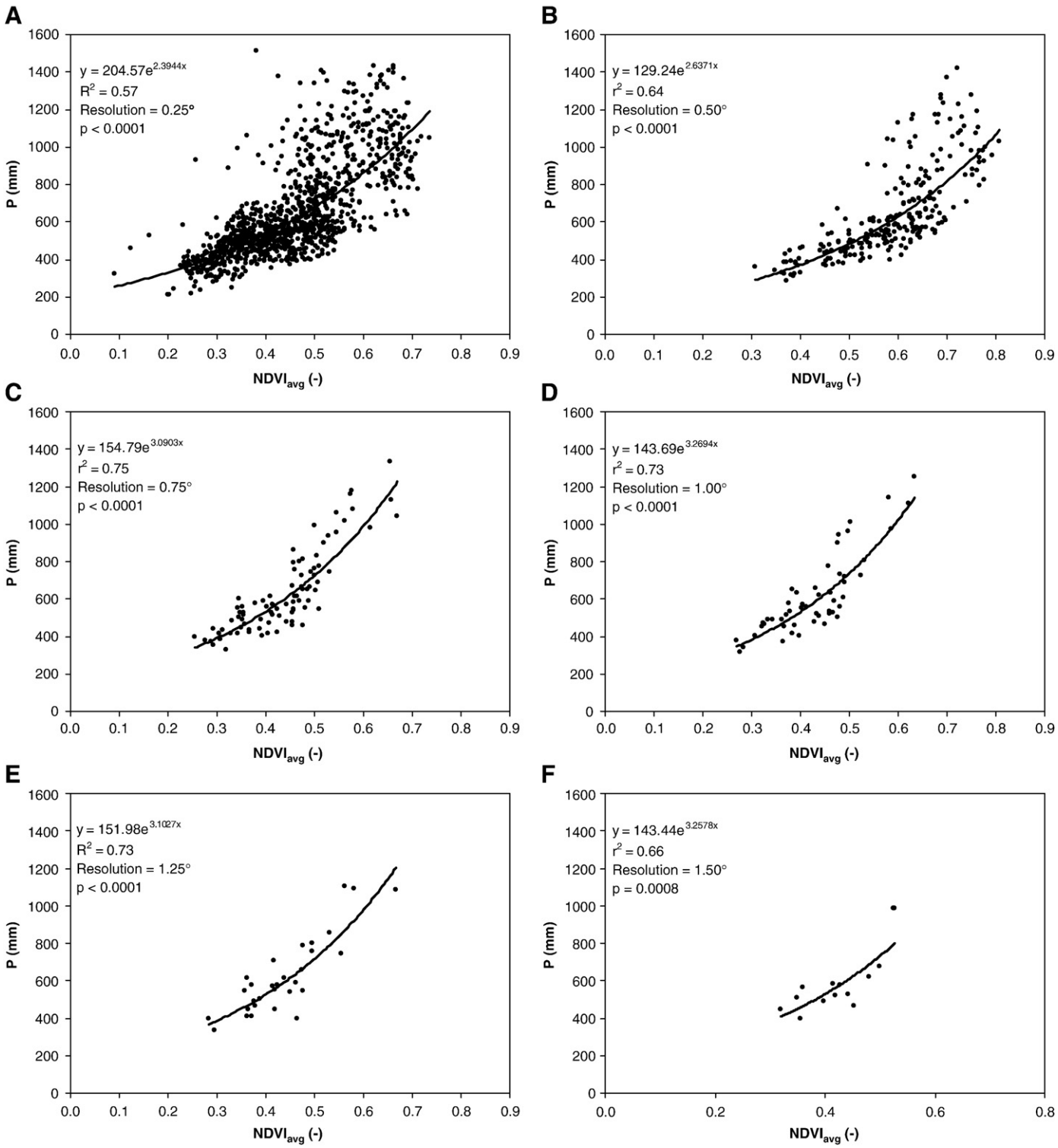

Fig. 4. Fitting of average annual NDVI and 3B43 accumulated annual precipitation (2001–2007) at different resolutions (0.25° (A), 0.50° (B), 0.75° (C), 1.00° (D), 1.25° (E) and 1.50° (F)).

and 3B43 obviously exists at different spatial scales. In other words, the greenness of vegetation, as reflected by the NDVI, is a function of different variables, including precipitation. By investigating the scale dependency of the precipitation-NDVI relation we isolated the NDVI response to precipitation in the best possible way. It is also acknowledged that both NDVI and TRMM do not provide perfect measurements and both are subject to bias due to orbital deviations, atmospheric conditions and imperfect retrieval algorithms. The scale dependency could be related to these factors as well.

4.2. Downscaling

Based on this analysis we used the following equation to calculate the NDVI based precipitation estimate at the 0.75° resolution

$$P_e(\mathrm{NDVI_{LR}}) = 154.8 \cdot e^{3.1 \cdot \mathrm{NDVI_{LR}}} \quad (7)$$

From Eq. (7) the low resolution NDVI based precipitation estimate was calculated. The result is shown in the top left map of Fig. 5. The

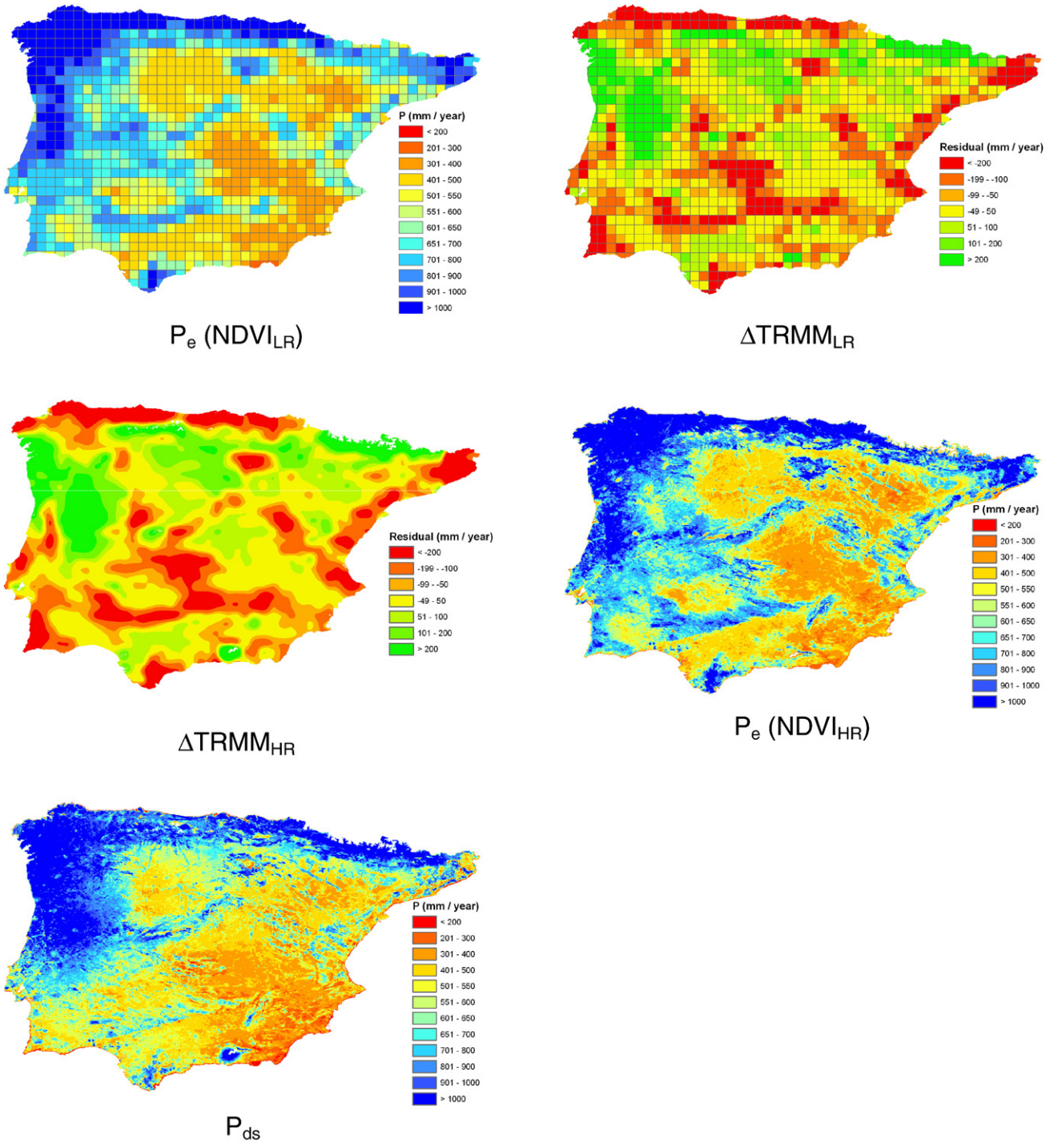

Fig. 5. Overview of the downscaling results: the low resolution NDVI based precipitation map (P_e (NDVI$_{LR}$)), the low resolution residual (ΔTRMM$_{LR}$), the high resolution residual (ΔTRMM$_{HR}$), the high resolution NDVI based precipitation map (P_e (NDVI$_{HR}$)), and the final downscaled precipitation map (P_{ds}) at 1 km resolution.

general precipitation patterns are well captured in this estimate. The north western part of Portugal, the Atlantic coast and the mountain ranges clearly are wetter and the estimated amounts correspond well with the 3B43 precipitation (bottom map of Fig. 3). However, for some regions substantial residuals are found after subtracting P_e from the 3B43 precipitation (top right of Fig. 5). This residual map represents that part of the precipitation that cannot be explained by NDVI alone. Negative residuals (red) indicate areas which are greener than expected, given the precipitation. These areas may possibly have an additional water source (irrigation, accumulated runoff, and groundwater) or are characterized by vegetation types less responsive to precipitation (for example evergreen needle forest with deep rooting systems). Positive residuals (green) depict areas that are less green than would be expected, given the observed precipitation. Steep and sparsely vegetated slopes in mountain ranges or areas with a high

Table 1
Validation results for downscaling of the average 2001–2007 precipitation

	P_{ds}	P_{3B42}	P_{3B43}
r^2	0.77	0.49	0.39
Bias	−0.01	−0.07	0.09
RMSE (mm)	120	173	201

Validation results are also shown for 3B42 and 3B43 TRMM data products at original resolution of 0.25°.

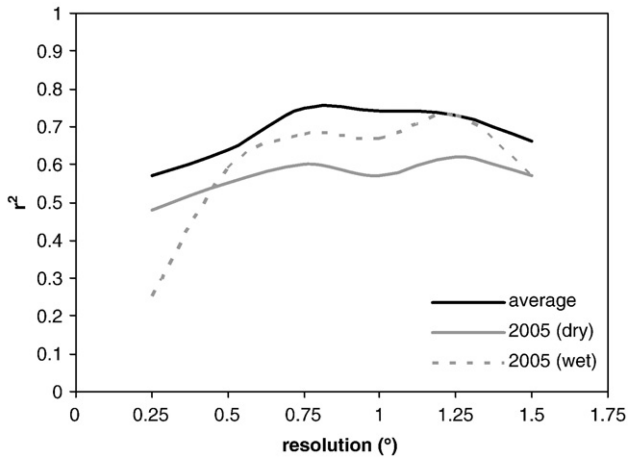

Fig. 6. Relation between resolution, and r^2 of NDVI regressed against 3B43 for a wet year (2003), a dry year (2005) and the average of 2001–2007.

precipitation that fall into the (over)saturated part of the NDVI-3B43 fit, could explain these residuals. The middle left figure shows the downscaled residuals using interpolation through the centre points of the 3B43 cells ($\Delta TRMM_{LR}$). The high resolution residual is interpolated from the 3B43 points using a minimum curvature spline technique. Future studies for improvements of the downscaling procedure should evaluate other interpolation techniques such as kriging or spatial autoregressive models. These techniques also allow inclusion of secondary information that could influence rainfall locally (e.g. relief, wind direction). The final downscaled precipitation map is the sum of $P_e(NDVI_{HR})$ and the downscaled residual ($\Delta TRMM_{HR}$) and is shown in the bottom left map of Fig. 5. This map now shows excellent agreement with the LR TRMM map, but with a much higher spatial resolution.

4.3. Validation

The efficacy of this method to improve precipitation mapping was validated using the ECA dataset. Out of the 28 ECA stations on the IP a total of 16 stations had a complete record of data from 2001–2007. These stations were used in the validation. The original low resolution 3B42, the 3B43 and the P_{ds} precipitation are extracted at the station locations and the validation indicators were calculated. The results of the validation are shown in Table 1. It can be concluded that the downscaling procedure has significantly increased the r^2 and reduced bias and RMSE. The downscaled precipitation map is of higher accuracy than the original 3B43 estimate and the downscaling approach is very promising. Another striking feature, apparent from Table 1, is the fact that for the average 2001–2007 precipitation, the original low resolution 3B42 product outperforms 3B43. This is unexpected as the 3B43 product is a combined satellite and gridded gauge based product, while the 3B42 product is based on satellite data only. A possible explanation could be that over a multi-year period the bias is reduced and the satellite data captures spatial heterogeneity better than the combined 3B43 product. It should also be acknowledged that Spain is near the outer limits of TRMM data acquisition. At these latitudes, the sampling errors can be relatively large.

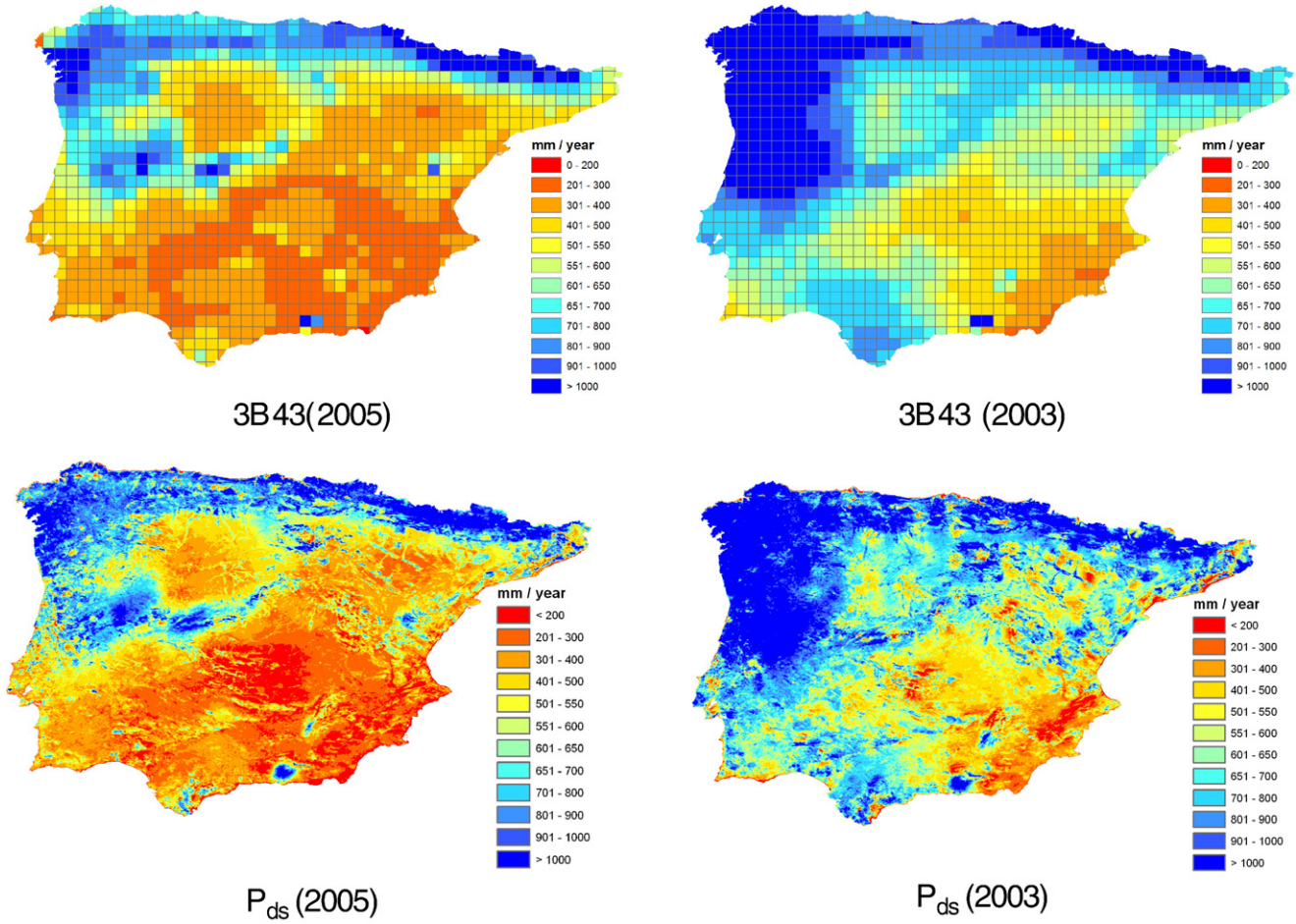

Fig. 7. 3B43 TRMM precipitation at nominal resolution of 0.25° and downscaled precipitation maps at 1 km resolution for the dry year (2005) and the wet year (2003).

Table 2
Validation results for downscaling of the 2003 (wet) and 2005 (dry) precipitation

		P_{ds}	P_{3B42}	P_{3B43}
2003	r^2	0.78	0.47	0.60
	Bias	−0.01	−0.23	0.05
	RMSE (mm)	188	331	248
2005	r^2	0.95	0.70	0.69
	Bias	−0.03	−0.18	−0.02
	RMSE (mm)	70	194	166

Validation results are also shown for 3B42 and 3B43 TRMM data products at original resolution of 0.25°.

Having shown successful downscaling for a multi-year average, the robustness of the method was tested for individual years. From the 2001–2007 time series the wettest year and driest year were selected. The average 2001–2007 3B43 precipitation equalled 650 mm, the year 2005 was the driest at 496 mm, and 2003 was the wettest at 745 mm. The methodology for 2003 and 2005 was similar to the one used in the case of average rainfall. First, the scale dependency was tested. Fig. 6 shows how r^2 varies with resolution for the average period from 2001–2007, for the dry year 2005 and for the wet year 2003. The coefficient of determination is, not surprisingly, highest for the average case. The variation in r^2 is highest in the wet year 2003, and the highest r^2 is found at a resolution of 1.25 (0.73). In the dry year the r^2 is highest at the same resolution, but slightly lower (0.62) than in the wet year. Other stress factors besides water shortage that cause reduced vegetation growth (e.g. temperature stress) could be a possible explanation.

The exponential function selected at the resolution where the r^2 is highest for 2005 (1.25°) is as follows

$$P_e(\mathrm{NDVI_{LR}}) = 104.9 \cdot e^{3.5 \cdot \mathrm{NDVI_{LR}}} \quad (8)$$

and for 2003 (1.25°) is as follows

$$P_e(\mathrm{NDVI_{LR}}) = 152.0 \cdot e^{3.1 \cdot \mathrm{NDVI_{LR}}} \quad (9)$$

There is notably a considerable lower coefficient of determination for the dry year 2005. Fig. 7 shows the downscaled precipitation maps for 2003 and 2005. The year 2005 was an extremely dry year, specifically in the southern part. There were extensive areas which received less than 300 mm rainfall, which in combination with reference evapotranspiration of nearly 1500 mm has led to extreme drought stress. The year 2003 obviously was much wetter. The area along the northern Atlantic coast is notably consistently wet, while the area along the south-western Mediterranean coast is extremely dry in both years. The other parts of the IP, specifically the inland areas, show a larger variation in annual precipitation.

From the 28 stations of the ECA dataset, stations with a full year of data for 2003 and 2005 respectively were selected for validation purposes. For 2003 19 stations were available and for 2005 20 stations were used and the validation results are presented in Table 2. These results confirm those from the multi-year average and the downscaling leads to improved r^2 and a reduced bias and RMSE. The r^2 was highest for the dry year, and the RMSE was also much lower than in the case of the wet or average year (70 mm). For these individual years the original low resolution 3B43 performed better than 3B42 with respect to bias and RMSE as can be expected. For both years there was a strong negative bias, e.g. the satellite estimates were significantly lower than the observed precipitation.

5. Conclusions

This study investigated downscaling of TRMM precipitation estimates on the Iberian Peninsula using a time series of TRMM 3B43 monthly precipitation products and SPOT VEGETATION 10-day NDVI imagery from 2001 to2007. A scale dependent exponential relation between precipitation and NDVI was used to develop a downscaling procedure and the results were validated using precipitation gauge data. A number of conclusions can be drawn based on this work:

- NDVI is a proxy for precipitation and on an annual basis an exponential function best describes this relationship.
- The correlation between precipitation and NDVI varies with resolution and the best correlations are found at a resolution of approximately 100 km (0.75°–1.25°). The highest r^2 was displayed by the regression fits for the 2001–2007 average precipitation and equalled 0.75.
- The downscaling approach resulted in very significant improvements in the accuracy and spatial resolution of the average 2001–2007 precipitation and for the annual precipitation of 2003 (wet) and 2005 (dry).
- We have refined the downscaling methodology as described by Agam et al. (2007) by selecting the basis function at an optimum resolution and by interpolating the residuals.
- The original low resolution 3B42 product outperforms the 3B43 product in the multi-year average precipitation analysis.
- We showed that it is feasible to increase spatial resolution and accuracy of precipitation estimates using vegetation greenness as a proxy for precipitation on an annual basis. Future work should focus on extending this procedure at a better temporal resolution (e.g. seasonal or monthly).
- On the IP the best relation between NDVI and precipitation is found at an approximate scale of 75–100 km. This is an intermediate scale and at smaller scales NDVI is probably determined primarily by anthropogenic land use. At larger scales factors such as geology, soils, and temperature may play an increasingly important role in explaining NDVI.

The main conclusion of this study is that it is possible to accurately downscale TRMM precipitation using vegetative response on the Iberian Peninsula and that the presented approach is generic in nature and is applicable in other semi-arid areas of the world.

Acknowledgements

This study was financially supported by Netherlands Agency for Aerospace Programmes (NIVR) through the Pre-qualification ESA Programs (PEP) subsidy scheme.

References

Adler, R. F., Kidd, C., Petty, G., Morissey, M., & Goodman, H. M. (2001). Intercomparison of Global Precipitation Products: The Third Precipitation Intercomparison Project (PIP-3). *Bulletin of the American Meteorological Society*, *82*, 1377–1396.

Agam, N., Kustas, W. P., Anderson, M. C., Li, F., & Neale, C. M. U. (2007). A vegetation index based technique for spatial sharpening of thermal imagery. *Remote Sensing of Environment*, *107*, 545–558.

Davenport, M. L., & Nicholson, S. (1993). On the relationship between rainfall and the Normalized Difference Vegetation Index for diverse vegetation types of East Africa. *International Journal of Remote Sensing*, *14*, 2369–2389.

Eckstein, B. A. (1989). Evaluation of spline and weighted average interpolation algorithms. *Computers & Geosciences*, *15*, 79–94.

Franke, R. (1982). Smooth interpolation of scattered data by local thin plate splines. *Computers and Mathematics with Applications*, *8*, 237–281.

Goodrich, D. C., Faures, J. M., Woolhiser, D. A., Lane, L. J., & Sorooshian, S. (1995). Measurements and analysis of small-scale convective storm rainfall variability. *Journal of Hydrology*, *173*, 283–308.

Grist, J., Nicholson, S. E., & Mpolokang, A. (1997). On the use of NDVI for estimating rainfall fields in the Kalahari of Botswana. *Journal of Arid Environments*, *35*, 195–214.

Guo, J., Liang, X., & Leung, L. R. (2004). Impacts of different precipitation data sources on water budgets. *Journal of Hydrology*, *298*, 311–334.

Hoffmann, L., El Idrissi, A., Pfister, L., Hingray, B., Guex, F., Musy, A., Humbert, J., Drogue, G., & Leviandier, T. (2004). Development of regionalized hydrological models in an area with short hydrological observation series. *River Research and Applications*, *20*, 243–254.

Huffman, G. J., Adler, R. F., Arkin, P., Chang, A., Ferraro, R., Gruber, A., Janowiak, J., McNab, A., Rudolf, B., & Schneider, U. (1997). The global precipitation climatology project (GPCP) combined precipitation dataset. *Bulletin of American Meteorological Society*, *78*, 5–20.

Huffman, G. J., Adler, R. F., Bolvin, D. T., Gu, G., Nelkin, E. J., Bowman, K. P., Hong, Y., Stocker, E. F., & Wolff, D. B. (2007). The TRMM Multisatellite Precipitation Analysis (TMPA): quasi-global, multiyear, combined-sensor precipitation estimates at fine scales. *Journal of Hydrometeorology*, *8*, 38–55.

Hutchinson, M. F., & Gessler, P. E. (1994). Splines — more than just a smooth interpolator. *Geoderma*, *62*, 45–67.

Immerzeel, W. W., Quiroz, R. A., & Jong de, S. M. (2005). Understanding complex spatiotemporal weather patterns and land use interaction in the Tibetan Autonomous Region using harmonic analysis of SPOT VGT-S10 NDVI time series. *International Journal of Remote Sensing*, *26*, 2281–2296.

Klein Tank, A. M. G., et al. (2002). Daily dataset of 20th-century surface air temperature and precipitation series for the European Climate Assessment. *International Journal of Climatology*, *22*, 1441–1453.

Kustas, W. P., Norman, J. M., Anderson, M. C., & French, A. N. (2003). Estimating subpixel surface temperatures and energy fluxes from the vegetation index-radiometric temperature relationship. *Remote Sensing of Environment*, *85*, 429–440.

Krajewski, W. F., & Smith, J. A. (2002). Radar hydrology: rainfall estimation. *Advances in water resources*, *25*, 1387–1394.

Malo, A., & Nicholson, S. E. (1990). A study of rainfall and vegetation dynamics in the African Sahel using Normalized Difference Vegetation Index. *Journal of Arid Environment*, *19*, 1–24.

Orlanski, I. (1975). A rational subdivision of scales for atmospheric processes. *Bulletin of the American Meteorological Society*, *56*, 527–530.

Pelgrum, H. 2000. Spatial aggregation of land surface characteristics: Impact of resolution of remote sensing data on land surface modelling. PhD thesis Wageningen University. Wageningen.

Rahman, H., & Dedieu, G. (1994). SMAC: A simplified method for the atmospheric correction of satellite measurements in the solar spectrum. *International Journal of Remote Sensing*, *15*, 123–143.

Rodriguez-Puebla, C., Encinas, A. H., Nieto, S., & Garmendia, J. (1998). Spatial and temporal patterns of annual precipitation variability over the Iberian Peninsula. *International Journal of Climatology*, *18*, 299–316.

Rudolf, B. (1993). Management and analysis of precipitation data on a routine basis. *Proc. Int. MO/IAHS/ETH Symp. on Precipitation and Evaporation, Bratislava, Slovakia, Slovak Hydromet. Inst.* (pp. 69–76).

Schuurmans, J. M., & Bierkens, M. F. P. (2007). Effect of spatial distribution of daily rainfall on interior catchment response of a distributed hydrological model. *Hydrology and Earth System Sciences*, *11*, 677–693.

Smith, M. B., Koren, V. I., Zhang, Z., Reed, S. M., Pan, J. J., & Moreda, F. (2004). Runoff response to spatial variability in precipitation: an analysis of observed data. *Journal of Hydrology*, *298*, 267–286.

Tucker, C. J. (1979). Red and photographic infrared linear combination for monitoring vegetation. *Remote Sensing of Environment*, *8*, 127–150.